


Research Paper

Near-infrared Intraoperative Imaging of Thoracic Sympathetic Nerves: From Preclinical Study to Clinical Trial

Kunshan He^{1, 2, 4*}, Jian Zhou^{1*}, Fan Yang^{1*}, Chongwei Chi^{2, 3}, Hao Li¹, Yamin Mao^{2, 3}, Bengang Hui¹, Kun Wang^{2, 3}, Jie Tian^{2, 3, 4, 5}, Jun Wang¹

1. Department of Thoracic Surgery, Peking University People's Hospital, No.11, Xi Zhi Men South Avenue, Beijing100190, China;
2. CAS Key Laboratory of Molecular Imaging, Institute of Automation, Chinese Academy of Sciences, Beijing 100190, China;
3. Beijing Key Laboratory of Molecular Imaging, Beijing 100190, China;
4. University of Chinese Academy of Sciences, Beijing 100039, China.
5. CAS Center for Excellence in Brain Science and Intelligence Technology, Institute of Automation, Chinese Academy of Sciences, Beijing, China.

* These authors contributed equally to this manuscript

 Corresponding author: Dr. Kun Wang, Email: kun.wang@ia.ac.cn Or Dr. Jie Tian, E-mail: tian@ieee.org; jie.tian@ia.ac.cn Or Dr. Jun Wang, Email: jwangmd@yahoo.com

© Ivyspring International Publisher. This is an open access article distributed under the terms of the Creative Commons Attribution (CC BY-NC) license (<https://creativecommons.org/licenses/by-nc/4.0/>). See <http://ivyspring.com/terms> for full terms and conditions.

Received: 2017.08.14; Accepted: 2017.10.02; Published: 2018.01.01

Abstract

The sympathetic nervous system controls and regulates the activities of the heart and other organs. Sympathetic nervous system dysfunction leads to disease. Therefore, intraoperative real-time imaging of thoracic sympathetic nerves (ITSN) would be of great clinical significance for diagnosis and therapy. The aim of this experimental study was to evaluate the feasibility and validity of intraoperative ITSN using indocyanine green (ICG).

Methods: ITSN using ICG was performed on 10 rabbits to determine its feasibility. Animals were allocated to two groups. The rabbits in one group received the same dose of ICG, but were observed at different times. The rabbits in the other group were administered different doses of ICG, but were observed at the same time. Signal to background ratio (SBR) was measured in regions of interest in all rabbits. Furthermore, fifteen consecutive patients with pulmonary nodules were intravenously injected with ICG 24 h preoperatively and underwent near-infrared (NIR) fluorescence imaging (FI) thoracoscopic surgeries between July 2015 and June 2016. A novel self-developed NIR and white-light dual-channel thoracoscope system was used. SBRs of thoracic sympathetic nerves were calculated in all patients.

Results: In the preclinical study, we were able to precisely recognize each rabbit's second (T2) to fifth (T5) thoracic ganglia on both sides of the spine using ITSN with ICG. In addition, we explored the relationship between SBR and the injection time of ICG and that between SBR and the dose of ICG. Using the novel dual-channel thoracoscope system, we were able to locate the ganglia from the stellate ganglion (SG) to the sixth thoracic ganglion (T6), as well as the chains between these ganglia in all patients with a high SBR value of 3.26 (standard deviation: 0.57). The pathological results confirmed our findings.

Conclusion: We were able to use ICG FI to distinguish thoracic sympathetic nerves during NIR thoracoscopic surgery. The technique may replace the rib-oriented method as standard practice for mapping the thoracic sympathetic nerves.

Key words: near-infrared; intraoperative fluorescence imaging; thoracoscopic surgery; sympathetic nerves; indocyanine green.

Introduction

The sympathetic nervous system regulates the balance in many homeostatic mechanisms, such as gut motility and pupil diameter, and is responsible for priming the body for action, particularly in dangerous situations. Moreover, sympathetic system stimulation causes vasoconstriction of most blood vessels. So thoracic sympathetic nerves, as important parts of sympathetic system, are involved in the treatment of multiple diseases. Currently, endoscopic thoracic sympathectomy is indicated mainly for primary hyperhidrosis, especially that of the palm [1], axilla, and the face [2,3]. Despite the development of modern pharmacological and endovascular treatments, sympathetic surgery still plays a critical role in the treatment of specific cardiac conditions, such as angina [4], long QT syndrome [5], and ventricular tachycardia [6]. In addition, thoracic sympathetic ablation is indicated for a few painful conditions and ischemia, such as pancreatic pain [7], complex regional pain syndrome [8], Raynaud's phenomenon [9], and digital ischemia [10,11]. Therefore, accurate intraoperative recognition of the thoracic sympathetic nerves is critical for the treatment of related diseases and for the development of new therapies.

Although the slender white-colored sympathetic chain often can be seen underneath the parietal pleura paralleling the vertebral column and above the heads of the ribs, its size and width are variable. In addition, its cephalad-caudal course may be meandering or straight. So far, no ganglion has clearly been visualized [12]. Although there are several anatomic landmarks that surgeons use as guides to identify the thoracic sympathetic chain or ganglion during surgery, the International Society on Sympathetic Surgery and the Society of Thoracic Surgeons recommend using a rib-oriented nomenclature [2]. In general, each thoracic ganglion lies in the intercostal space between its corresponding ribs and is referred to based on the anatomical structure. Therefore, surgeons indirectly and roughly determine the locations of the ganglia by counting the ribs at the time of surgery. However, this method has some limitations. Some studies have confirmed that anatomic variations often cause changes in the corresponding spatial locations between thoracic ganglia and the ribs. For example, Street *et al.* found in their series that 6.25% of ganglia were located below their associated intercostal spaces rather than within their corresponding intercostal space. In addition, the stellate ganglion (SG), which was formed by the inferior cervical ganglion and the first thoracic ganglion (T1), was present in only 70% of specimens [13]. Chung *et al.* have reported that the SG and the second thoracic ganglion (T2) are fused in

9.1% of patients [14]. Failure in the accurate identification of thoracic ganglia may result in operation failure and severe complications [2, 15].

Fluorescence imaging (FI) is a novel intraoperative imaging modality used to help guide the surgeon in the detection of benign and/or malignant tissues [16], and has been used for the detection and treatment of multiple diseases, such as ovarian cancer using specific FI [17], head and neck cancer [18] and peritoneal carcinomatosis from colorectal cancer [19,20] using non-specific FI. However, only a few FI studies of nerves in the clinical have been reported. Wagner *et al.* identified the contralateral pericardiophrenic neurovascular bundle by fluorescing the pericardiophrenic vessels during robotic thymectomy [21]. Chen *et al.* recognized facial nerve by highlighting the vessels inside the vasa nervorum during mastoidectomy [22]. Our team first reported that thoracic ganglia can be directly visualized during thoracoscopic indocyanine green (ICG) fluorescence guided surgery (ICG-FGS) in a case report [23,24]. Notably, ICG has been authorized by the Food and Drug Administration (FDA) for determining cardiac output, hepatic function and liver blood flow, and for ophthalmic angiography.

In this study, we firstly evaluated the feasibility of intraoperative real-time imaging of thoracic sympathetic nerves (ITSN) with ICG and explored the relationship between the signal to background ratio (SBR) and the injection time of ICG and that between SBR and the dose of ICG using a rabbit model. Because sympathetic nerves were subtle and difficult to detect, a fluorescence microscope system was developed. Then, to study the validity of this method, we carried out a clinical trial with our self-developed near-infrared (NIR) and white-light dual-channel thoracoscope system in Peking University People's Hospital.

Materials and Methods

Fluorescence Microscope System

We developed a modified fluorescence microscope system (Fig. 1A) in-house. Briefly, a traditional stereomicroscope (Leica M205 FA, Germany) was coupled with a color camera and an NIR scientific complementary metal-oxide-semiconductor (SCMOS) camera (pco.edge 5.5 m). An NIR laser source (center wavelength: 785 nm, maximum power: 800 mW) was combined with an optical filter module installed in the stereomicroscope through a uniform fiber, so that a specified wavelength of light was transmitted onto the imaging target. The emission light radiated by the excited fluorophore

was first filtered by the filter module and then captured by the NIR camera. Similarly, the color camera captured visible images illuminated by the light emitting diode. This system was able to produce a strong and noise-free fluorescence image against the background and a bright and high-resolution visible image.

Fluorescence Endoscopic Imaging System

The NIR (800-900 nm) and white-light (400-650 nm) dual-channel thoracoscope system was developed by the Key Laboratory of Molecular Imaging of the Chinese Academy of Sciences on the basis of our previous studies [25-29]. A picture of the novel system is presented in Fig. 3A. Briefly, the system consisted of four modules: the light-source module, the detector module, the control module, and the display module. The spatial resolution of the system was 35 μm and the minimal detectable ICG concentration was 0.01 μM .

In addition to the ergonomic improvements compared to our previous system [27], the novel system used a custom prism with a 30° viewing angle. The use of this prism not only made probing the thoracic sympathetic nerve more convenient, but also resulted in a large aperture and a wide field. Due to the presence of high levels of noise and the weak fluorescence signal during this experiment, we designed a new image enhancement algorithm to improve the qualities of the color and fluorescence images. This system also had improved quantitative analysis functionality, which enabled us to perform the quantitative statistical analysis of the fluorescence intensity and the calculation of SBR in real-time. The quantification techniques of fluorescence intensity signal included fluorescence signal extraction based on fuzzy C-mean clustering and level-set algorithms, fluorescence intensity distribution analysis, the radiometric calculation of fluorescence image and other conventional image analysis methods.

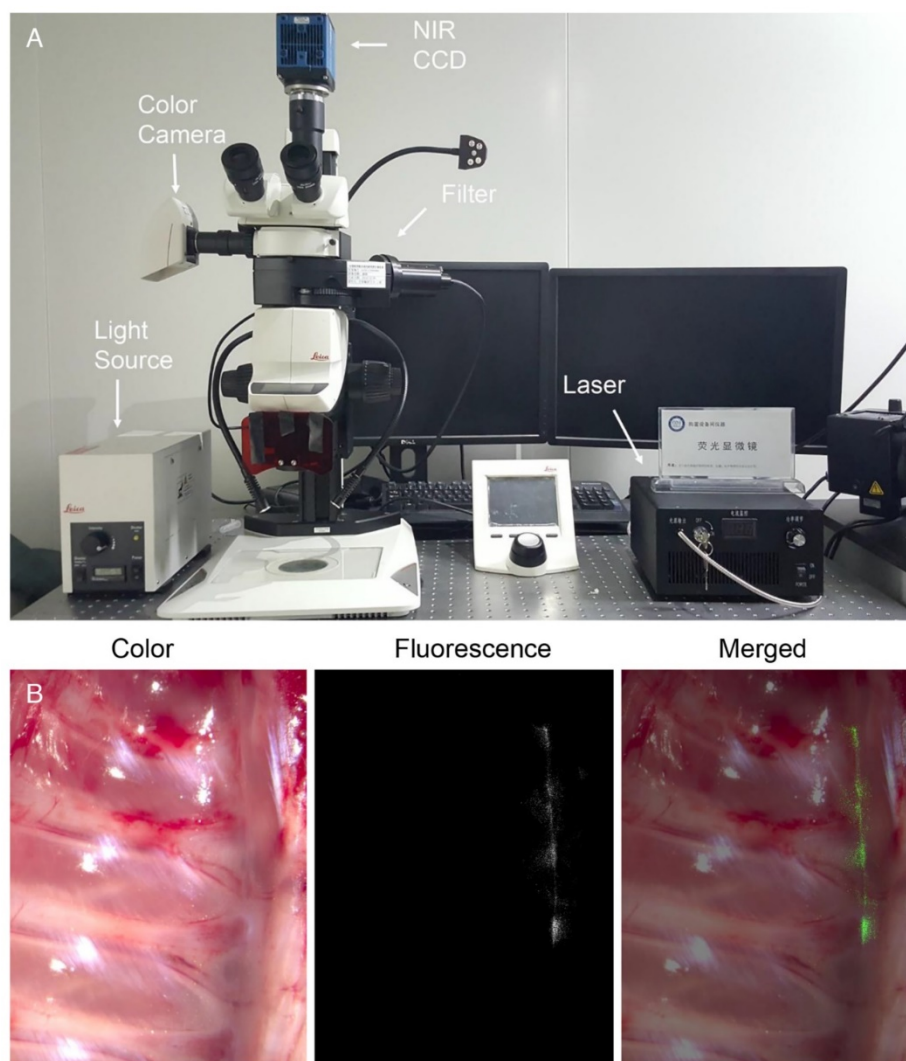


Figure 1. (A) Photograph of the modified fluorescence microscope system. (B) *Ex vivo* imaging of the rabbit's thoracic sympathetic nerve, including color, fluorescence, and merged images. NIR CCD: near-infrared charge-coupled device.

Animals

Four male and six female Japanese white rabbits (weight: 1.75-2.4 kg, average: 2.15 kg) were purchased from Beijing Vital River Laboratory Animal Technology Co., Ltd. (China). The Institutional Animal Care and Use Committee of Peking University People's Hospital approved this animal study. To obtain the relationship between SBR and the injection time of ICG and that between SBR and the dose of ICG, we allocated the ten rabbits to two groups. One group was the dose group and the other group was the timing group.

Patients

The subjects comprised 15 eligible patients who were scheduled for video-assisted thoracoscopic surgery at Peking University People's Hospital between July 2015 and June 2016. The characteristics of the patients are shown in Table 1. The inclusion criteria were as follows: age between 18 and 75, pulmonary nodules scheduled for thoracoscopy or thoracotomy, preoperatively normal liver function, no ICG or iodine allergies, negative findings on an ICG skin test, volunteering to participate in this study, and providing signed informed consent. The exclusion criteria were preoperative liver dysfunction, ICG or iodine allergies, positive results on an ICG skin test, other well-controlled comorbidities, and being deemed unsuitable for enrolment by the clinicians.

Before surgery, all patients were diagnosed with pulmonary nodules using high-resolution computed tomography with 1 mm slice thickness. All patients provided signed informed consent. The Peking University People's Hospital Institutional Review Board authorized this study (2015PHB157-01). The Clinical Trials number for the study is NCT02611245.

Administration of Contrast Agents

ICG (25 mg vials) was purchased from Tianyi Pharmaceutical Co., Ltd. (Liaoning, China). First, the rabbits in the timing group were injected with 10 mg/kg ICG in sterile water for injection (SWI) 24, 22, 20, 18, and 16 h preoperatively through the marginal ear vein. After calculating the SBR for each time point, the rabbits in the dose group were then injected with 7, 8.5, 10, 11.5, and 13 mg/kg of ICG in SWI 20 h preoperatively.

For patients' safety reasons, we referred to several studies [30-34] in tumor identification for pulmonary nodules and brain tumors and then chose the ICG concentration of 5 mg/kg. Three patients were respectively injected 5 mg/kg ICG 16, 20 and 24 h preoperatively. Through observation, we determined 5 mg/kg and 24 h preoperatively was the best combination. Then 15 patients were

intravenously injected with 5 mg/kg of ICG 24 h preoperatively. No adverse reactions or allergic reactions were observed in any of the subjects.

Table 1. Characteristics of the 15 patients who participated in this study

Study no.	Age	Sex	BMI	History of allergy	Tumor size (cm)	Tumor location	Pathology
1	52	M	25.76	NO	1*0.5	RUL	ADE
2	33	F	20.07	NO	1.2*0.7	LLL	CRC
3	74	F	25.01	NO	0.7*0.6	LUL	ADE
4	44	F	23.44	NO	0.6*0.5	RUL	AIS
5	30	M	19.69	NO	2*1	RML	CHO
6	63	M	26.99	NO	2.5*2	RML	CCRCC
7	65	F	19.53	NO	1.5*1	RLL	AIS
8	43	F	23.62	YES	5*4	RLL	ADE
9	61	F	23.44	NO	3*2	LUL	HCC
10	57	F	20.03	NO	0.6*0.4	RUL	ADE
11	52	M	25.59	NO	4*3	LML	HCC
12	61	F	26.37	NO	2.5*2	RLL	ADE
13	52	M	22.68	NO	5*4	RLL	ADE
14	50	F	22.32	NO	5*3	LLL	ADE
15	67	F	20.83	NO	3.2*2.2	RUL	ADE

ADE: adenocarcinoma; AIS: adenocarcinoma *in situ*; CCRCC: clear cell renal cell carcinoma; CHO: chondrosarcoma; CRC: colorectal cancer; F: female; HCC: hepatocellular carcinoma; LLL: left lower lobe;

LML: left middle lobe; LUL: left upper lobe; M: male; RLL: right lower lobe; RML: right middle lobe; RUL: right upper lobe

Preclinical Imaging Procedure

After routine injection of ICG preoperatively, the rabbits were injected with 6 mg/kg of 0.7% sodium pentobarbital solution in the marginal ear vein. Upon disappearance of the corneal reflex, the rabbits were executed by injection of 50 mL of air through veins. A median thoracotomy was performed. The lung, heart, and aorta were then dissected and removed. The sympathetic nerves on either side of the spine were exposed. Lastly, the spine was cut from the thoracic apex to the diaphragm, and the ribs were cut 3 cm from the spine. The entire chest wall with contact parietal pleura was removed. Then the specimens were washed using physiological saline solution.

The dissected specimens were placed on the microscope table. After adjustments of the appropriate imaging distance and field of vision, a color image was captured. We then switched the microscope to NIR mode, turned off all of the laboratory light sources, and obtained a fluorescence image. Finally, under the guidance of fluorescence signal, we carefully removed the ICG-stained thoracic sympathetic ganglia and the chains on both sides of the spine.

Clinical Imaging Procedure

After the scheduled injection of ICG, the patients were placed in a lateral position and underwent double-catheter trachea insertion under general

anesthesia. After routine disinfection, the thoracoscope was inserted at the seventh rib. Before the lung excision operation, the lung was pulled to the front and the posterior mediastinum was revealed. The sympathetic nerves were then explored from top to bottom. We determined and recorded the positions and fluorescence intensities of SG through T6 and the chains in between. Patient No. 11 was diagnosed with pulmonary nodules and posterior mediastinal tumor. After the lung nodules were removed, the mediastinal tumor and T3 were resected together, as they were too close to each other to separate. All excised specimens were then sent to the pathology department.

Histopathologic Assessment

All of the dissected specimens were fixed in 10% phosphate-buffered formalin for 24 h. Paraffin-embedded tissues were consecutively sliced at 5 μm intervals. First, the pathologist analyzed the unstained sections. The sections were then stained with hematoxylin-eosin (H&E) and examined according to the standard pathology protocol. This is because H&E staining may compromise the observation of the ICG fluorescence signal. Areas of the section with fluorescence signals merged with staining of the neurocyte were identified. In addition, we used tyrosine hydroxylase (TH) antibodies (Rabbit polyclonal anti-TH antibody, ab112, Abcam) to identify sympathetic ganglion cells and confirmed our findings [35].

Statistical Analysis

SBR of thoracic sympathetic nerves were calculated by the method as follows: Firstly, we used ImageJ (Image processing Software, National Institutes of Health, USA) to delineate ganglions or chains as a region of interest (ROI) and calculated the mean brightness value of ROI (V_{Signal}). Meanwhile, the surrounding background region was highlighted and the mean brightness value of this region ($V_{\text{Background}}$) was also measured. SBR values for each thoracic sympathetic ganglion or chain were calculated six times to reduce errors by dividing V_{Signal} by $V_{\text{Background}}$. The Kruskal-Wallis test was used to compare multiple independent samples. To maintain consistency in our calculations, we selected the bilateral second to fifth thoracic sympathetic ganglia (T2, T3, T4, and T5) and used their average value to denote each rabbit's SBR. We adopted this approach because the area and intensity of the NIR laser source were limited. Data analysis and graphing were performed using OriginPro 2016 (OriginLab Corporation, USA). P-values < 0.050 were considered statistically significant.

Results

Preclinical Study Results

The microscopic examinations enabled us to identify each rabbit's T2 to T5 ganglia (8 in total) on both sides of the spine. All of the sympathetic ganglia and the chains between them were identified using our FI method on the surface of the specimens. The areas with high SBR values in the fluorescence images matched the thoracic nerves as seen in the color images perfectly (Fig. 1B) and confirmed our findings. Shorter time intervals between the ICG injection and the operation led to stronger fluorescence signals in the rabbits in the timing group. However, the SBR for the rabbit injected with ICG 20 h preoperatively was the highest in the group ($p < 0.001$, Fig. 2A). In the dose group, larger doses of ICG led to stronger fluorescence signals. However, the SBR for the rabbit injected with 10 mg/kg of ICG was the highest in the group ($p < 0.001$, Fig. 2B). In the process of statistical analysis, n values of the number of samples are all equal to six.

Fluorescence microscopy confirmed the presence of fluorescence in the specimens (Fig. 2C), which were resected under the guidance of the fluorescence signal. We found large numbers of neurocytes in the areas with strong fluorescence signals (Fig. 2D). However, there were a few nerve cells in areas with weak fluorescence signals. We used pathological examination to verify our findings.

Clinical Trial Results

We used ITSN with ICG to successfully identify the thoracic sympathetic ganglia SG to T6 (12 in total) and the chains in between in each patient (Figs. 3B-D). The mean SBR value for all ganglia was 3.26 (standard deviation: 0.57), which was sufficiently high to assist the surgeons in identifying the ganglia during surgery. Moreover, the strong fluorescence signal lasted for longer than five hours. The calculated SBR values for SG through T6 for all subjects are shown in Fig. 4A. The SBR value for SG was the lowest ($p < 0.001$) and those for T2 to T6 were not significantly different from each other ($p > 0.050$). In the process of data statistics, n values of the number of samples are all equal to 30.

Fluorescence microscopy enabled us to find a strong fluorescence signal in the paraffin section from the thoracic sympathetic nerve specimen from patient No. 11 (Fig. 4B-D). The fluorescence was mainly distributed in areas with large numbers of nerve cells. H&E staining of the section confirmed our findings (Fig. 4E).

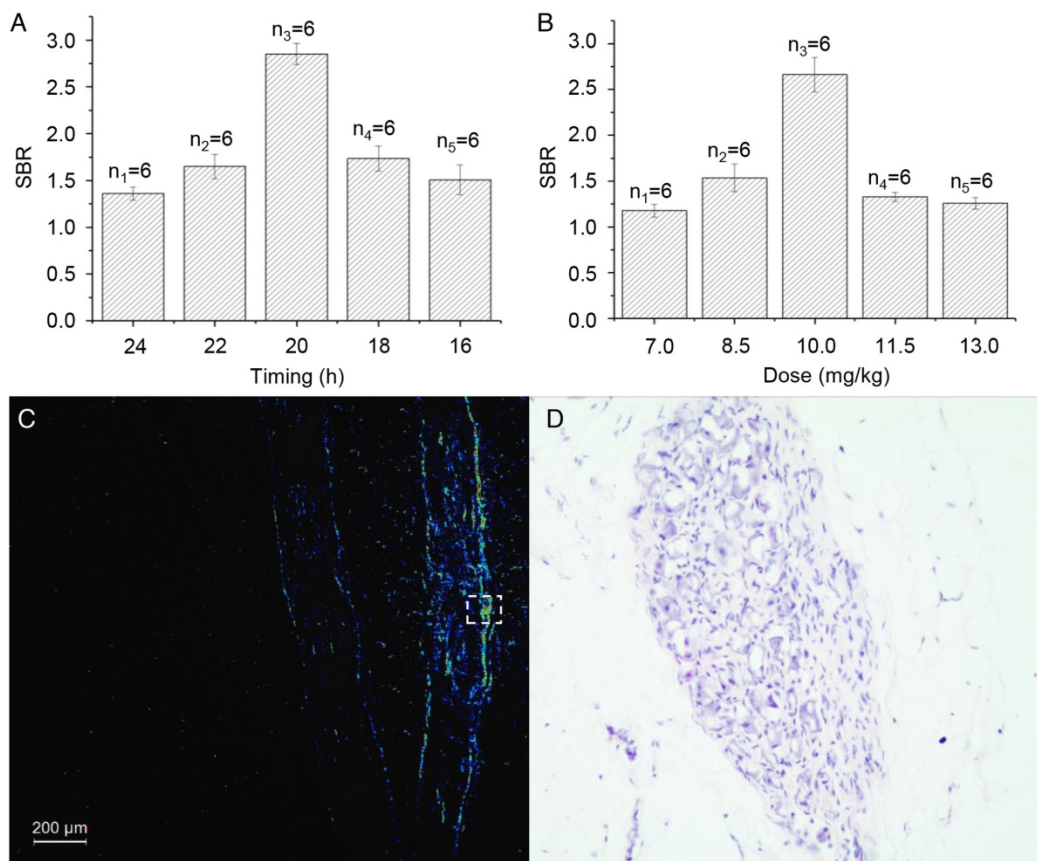


Figure 2. (A) The relationship between SBR and the injection time in each rabbit in the timing group. (B) The relationship between SBR and the dose of ICG in each rabbit in the dose group. (C) Representative fluorescence image of a paraffin section of a rabbit's thoracic sympathetic nerves. (D) H&E-stained cross-section of the area marked by the dotted box in Fig. 2C. SBR: signal to background ratio.

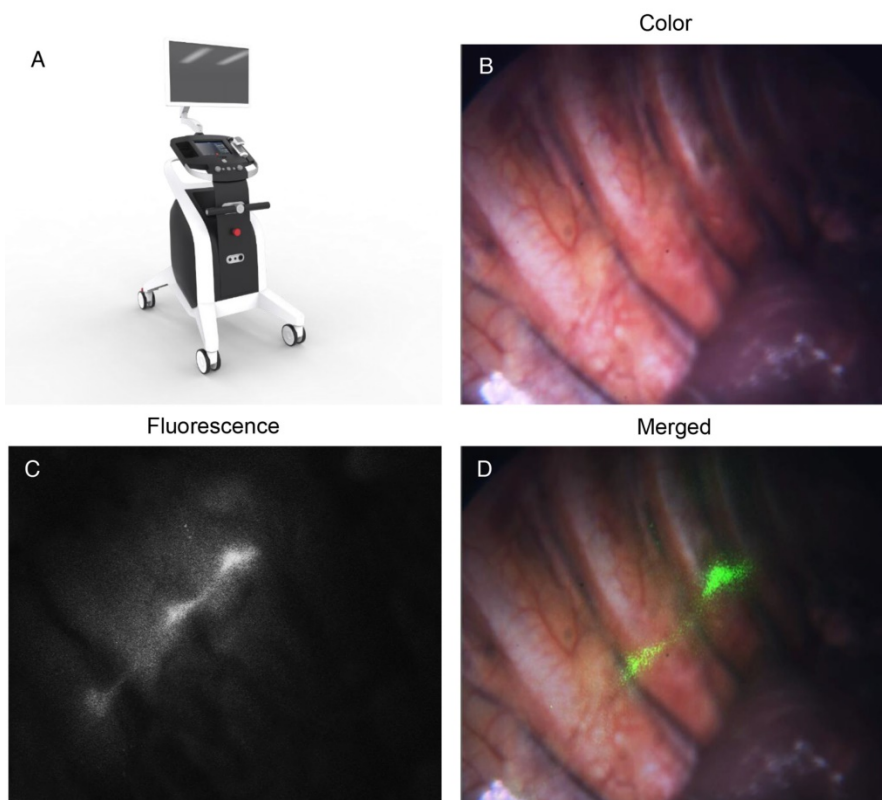


Figure 3. (A) A picture of the dual-channel thoracoscope system. (B-D) *In vivo* thoracic sympathetic nerve images of a patient, including color, fluorescence, and merged images.

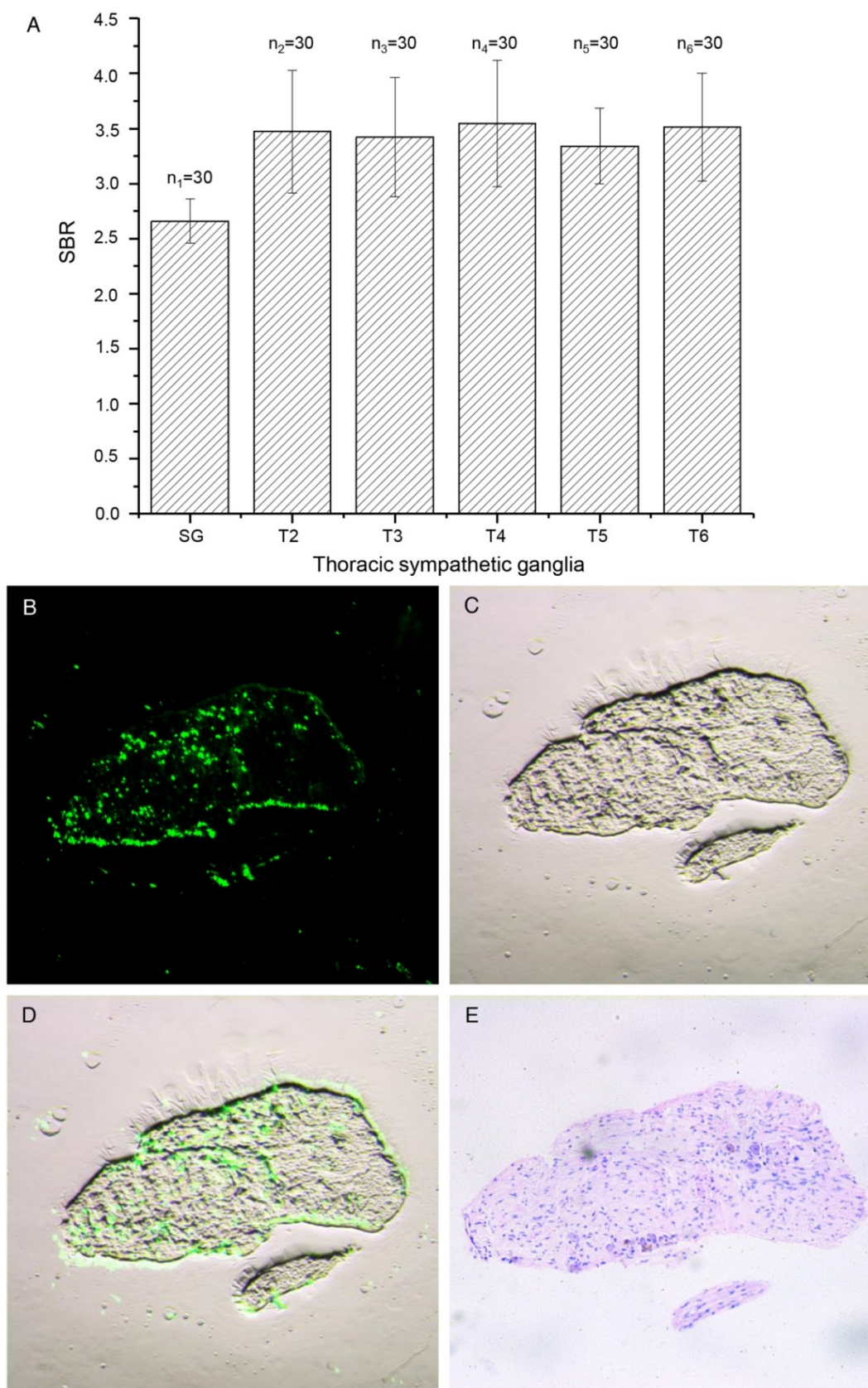


Figure 4. (A) The SBR values for SG to T6 for all patients. (B-D) Fluorescence, color and merged images of a paraffin section of the thoracic sympathetic nerve specimen from patient No. 11. (E) H&E-stained section of the area shown in Fig. 4C. SBR: signal to background ratio.

Discussion

Here we investigated the feasibility and validity of intraoperative ITSN with ICG in both a preclinical study and a clinical trial. We were able to identify T2 to T5 on both sides of the spine in each rabbit and obtained the relationship between SBR and the injection time of ICG and that between SBR and the dose of ICG in the preclinical study. The false-negative rate was 0% (0/10 rabbits). We used the method described here to successfully identify the thoracic sympathetic ganglia SG through T6 (12 in total) and the chains in between in each patient in the clinical study. High SBR values in ITSN with ICG highly depend on the ICG dose, imaging timing, and the sensitivity of the imaging system. Therefore, we developed a modified fluorescence microscope system and an NIR and white-light dual-channel thoracoscope system especially optimized for NIR light collection efficiency. The combination of intraoperative ITSN with ICG and the novel thoracoscope system displayed enormous potential in clinical application.

The novel method described here has several advantages when compared to traditional approaches. First, the high-SBR and intraoperative real-time imaging contributes to the objective and accurate identification of thoracic sympathetic nerves during surgery. Second, NIR light can penetrate much deeper into blood and tissue than visible light. In addition, autofluorescence is very weak in this spectral range. Lastly, this method is minimally invasive and does not interfere with the conventional surgical procedure. Moreover, no adverse reactions or allergic reactions occurred in this study.

ICG is a water-soluble compound with a molecular weight of 755 Da and has been clinically approved for longer than 60 years by the FDA. When injected into the human vein, it binds intensely to high-density lipoprotein and low-density lipoprotein [36]. Its half-life is 150-180 s. According to the National Cancer Institute, ICG is excreted from the circulation exclusively by the liver into bile. At first, ICG was mainly used to determine cardiac output and hepatic function. In 2009, Ishizawa *et al.* reported the presence of illuminated liver tumors using ICG [37]. These tumors emitted light that peaked at around 830 nm when excited with NIR light. Nowadays, ICG FI plays an important role in sentinel lymph node detection [38, 39], lymphedema diagnosis and management [40], tumor identification [41] and organ perfusion assessment [42]. In this study, we for the first time used ICG FI to identify the thoracic sympathetic nerves.

Based on the properties of ICG and our

preliminary studies, we believe that the high-SBR fluorescence signal from the thoracic sympathetic nerves may result from the specific structure of these nerves. There is a layer of connective tissue membrane containing blood vessels, nerves, and fat cells on the sympathetic ganglion surface. This later may lead to enhanced permeability and retention (EPR) of ICG, similar to certain types of cancer tissue [43, 44]. This phenomenon is more marked in humans than in rabbits, perhaps due to the larger sizes of the sympathetic nerves. Notably, the SBR value for the SG is lower than that for T2 through T6. This is because there is a fat pad in the hemithorax vertex that often covers the SG.

The EPR effect, firstly reported by Maeda *et al.*, is a property that protein-bound molecules and other nano-sized materials passively accumulate in tumors after systemic administration [45]. Ideally, nerve-specific contrast agents should be adopted during nerve-sparing FI surgery. Nowadays, Whitney *et al.* are utilizing NIR fluorescent peptides that bind to nerve sheaths to develop nerve-specific agents on rat model [46]. And Gibbs-Strauss *et al.* are developing nerve-specific agents based on small, hydrophobic molecules that bind to the myelin of neurons on animal model [47]. However, no clinical trial has ever been reported on nerve-specific contrast agents.

Structurally, thoracic sympathetic nerves are important parts of the sympathetic nervous system and have both white and gray matter rami communicates [48]. Functionally, thoracic sympathetic nerves provide sympathetic innervation to the internal organs of the chest. Intraoperative real-time ITSN is conducive to the preservation of the nerves during certain surgeries, such as mediastinal tumor surgery, which is equally crucial to achieving optimal prognosis [16]. In addition, ITSN is critical for the accurate ablation or resection of ganglia and chains and in the diagnosis and treatment of related diseases. Moreover, this technique has huge potential for the development of novel therapeutic modalities. In our future work, we will further optimize the dose of ICG and the sensitivity of our imaging system, and attempt to use this method to visualize other nerves.

Conclusion

In this study, we successfully identified thoracic sympathetic nerves using ITSN with ICG in both preclinical and clinical studies. Moreover, the relationship between SBR and the injection time of ICG and that between SBR and the dose of ICG were explored, and a novel NIR and white-light dual-channel thoracoscope system was developed. Pathological studies confirmed our findings. This new method may replace the rib-oriented method as

standard practice for the identification of the thoracic sympathetic nerves.

Abbreviations

FDA: Food and Drug Administration; FI: fluorescence imaging; H&E: hematoxylin-eosin; ICG: indocyanine green; ITSN: imaging of thoracic sympathetic nerves; NIR: near-infrared; ROI: region of interest; SBR: signal to background ratio; SG: stellate ganglion; SWI: sterile water for injection

Acknowledgments

This work was supported by the National Key Research and Development Program of China under Grant No. 2017YFA0205200 and 2016YFC0103702, the National Natural Science Foundation of China under Grant No. 81227901, 81527805, 61231004, 61501462 and 61671449, the International Innovation Team of CAS under Grant No. 20140491524, Beijing Municipal Science & Technology Commission No. Z161100002616022 and Peking University People's Hospital Research and Development Foundation (No. RDC2015-33).

All authors have read the journal's authorship agreement and the article has been reviewed by and approved by all named authors. Moreover, we thank Yun Wang and Fei Yang of Peking University People's Hospital for the help of pathological staining and analysis.

The clinical trial was registered using the name "NIR fluorescence imaging technique in thoracic surgery with ICG". The Clinical Trial number is NCT02084784.

Competing Interests

The authors have declared that no competing interest exists.

References

1. Hashmonai M, Licht PB, Schick CH, Bishop G, Cameron AEP, Connery CP, et al. Late results of endoscopic thoracic sympathectomy for hyperhidrosis and facial blushing (Br J Surg 2011; 98: 1719-1724). *Brit J Surg*. 2012; 99: 1719-24.
2. Cerfolio RJ, De Campos JR, Bryant AS, Connery CP, Miller DL, Decamp MM, et al. The Society of Thoracic Surgeons expert consensus for the surgical treatment of hyperhidrosis. *Ann Thorac Surg*. 2011; 91: 1642.
3. Nicholas R, Quddus A, Baker DM. Treatment of Primary Craniofacial Hyperhidrosis: A Systematic Review. *Am J Clin Dermatol*. 2015; 16: 361-70.
4. Abbate A, Hamza M, Cassano AD, Melchior R, Roberts C, Grizzard J, et al. Sympathectomy as a treatment for refractory coronary artery spasm. *Int J Cardiol*. 2012; 161: 7-9.
5. Schwartz PJ, Ackerman MJ. The long QT syndrome: a transatlantic clinical approach to diagnosis and therapy. *Eur Heart J*. 2013; 34: 3109-16.
6. Vaseghi M, Gima J, Kanaan C, Ajjola OA, Marmureanu A, Mahajan A, et al. Cardiac sympathetic denervation in patients with refractory ventricular arrhythmias or electrical storm: intermediate and long-term follow-up. *Heart Rhythm the Official Journal of the Heart Rhythm Society*. 2014; 11: 360.
7. Issa Y, Ahmed AU, Bouwense SA, van Santvoort HC, Van GH. Preoperative opioid use and the outcome of thoracoscopic splanchnicectomy in chronic pancreatitis: a systematic review. *Surgical Endoscopy*. 2014; 28: 405-12.
8. Agarwal-Kozlowski K, Lorke DE, Habermann CR, Schulte aEJ, Beck H. Interventional management of intractable sympathetically mediated pain by computed tomography-guided catheter implantation for block and

neuroablation of the thoracic sympathetic chain: technical approach and review of 322 procedures. *Anaesthesia*. 2011; 66: 699-708.

9. Landry GJ. Current medical and surgical management of Raynaud's syndrome. *J Vasc Surg*. 2013; 57: 1710-6.
10. Coveliers HME, Hoexum F, Nederhoed JH, Wisselink W, Rauwerda JA. Thoracic sympathectomy for digital ischemia: A summary of evidence. *J Vasc Surg*. 2011; 54: 273-7.
11. Hoexum F, Coveliers HM, Lu JJ, Jongkind V, Yeung K, Wisselink W. Thoracic sympathectomy for upper extremity ischemia. *Minerva Cardioangiol*. 2016; 64.
12. Krasna MJ, Flowers J, Morvick R. Thoracoscopic sympathectomy. *Surg Laparosc Endosc*. 2010; 20: 323-30.
13. Street E, Ashrafi M, Greaves N, Gouldsbrough I, Baguneid M. Anatomical variation of rami communicantes in the upper thoracic sympathetic chain: A human cadaveric study. *Ann Vasc Surg*. 2016; 34: 243-9.
14. Chung IH, Oh CS, Koh KS, Kim HJ, Paik HC, Lee DY. Anatomic variations of the T2 nerve root (including the nerve of Kuntz) and their implications for sympathectomy. *Journal of Thoracic & Cardiovascular Surgery*. 2002; 123: 498-501.
15. Hashmonai M, Cameron AEP, Licht PB, Hensman C, Schick CH. Thoracic sympathectomy: a review of current indications. *Surgical Endoscopy*. 2016; 30: 1255-69.
16. Nguyen QT, Tsien RY. Fluorescence-guided surgery with live molecular navigation—a new cutting edge. *Nature reviews Cancer*. 2013; 13: 653.
17. van Dam GM, Themelis G, Crane LM, Harlaar NJ, Pleijhuis RG, Kelder W, et al. Intraoperative tumor-specific fluorescence imaging in ovarian cancer by folate receptor- α targeting: first in-human results. *Nat Med*. 2011; 17: 1315.
18. Moore LS, Rosenthal EL, Chung TK, De BE, Patel N, Prince AC, et al. Characterizing the utilities and limitations of repurposing an open-field optical imaging device for fluorescence-guided surgery in head and neck cancer patients. *J Nucl Med*. 2016; 58.
19. Filippello A, Porcheron J, Klein JP, Cottier M, Barabino G. Affinity of Indocyanine Green in the Detection of Colorectal Peritoneal Carcinomatosis: The Role of Enhanced Permeability and Retention Effect. *Surg Innov*. 2016; 24.
20. Liberale G, Vankerckhove S, Caldron MG, Ahmed B, Moreau M, El Nakadi I, et al. Fluorescence imaging after indocyanine green injection for detection of peritoneal metastases in patients undergoing cytoreductive surgery for peritoneal carcinomatosis from colorectal cancer: a pilot study. *Ann Surg*. 2016; 264: 1110-5.
21. Wagner OJ, Louie BE, Vallières E, Aye RW, Farivar AS. Near-infrared fluorescence imaging can help identify the contralateral phrenic nerve during robotic thymectomy. *Ann Thorac Surg*. 2012; 94: 622-5.
22. Chen SC, Wang MC, Wang WH, Lee CC, Wang TF, Lin CF, et al. Fluorescence-assisted visualization of facial nerve during mastoidectomy: A novel technique for preventing iatrogenic facial paralysis. *Auris Nasus Larynx*. 2014; 42: 113-8.
23. Weng W, Liu Y, Zhou J, Li H, Yang F, Jiang G, et al. Thoracoscopic Indocyanine Green Near-Infrared Fluorescence for Thoracic Sympathetic Ganglions. *Ann Thorac Surg*. 2016; 101: 2394.
24. Zhou J, Yang F, Jiang G, Wang J. Applications of indocyanine green based near-infrared fluorescence imaging in thoracic surgery. *J Thorac Dis*. 2016; 8: S738.
25. Leng CC, Tian J. Mathematical method in optical molecular imaging. *Science China Information Sciences*. 2015; 58: 31101-031101.
26. Chi C, Du Y, Ye J, Kou D, Qiu J, Wang J, et al. Intraoperative imaging-guided cancer surgery: from current fluorescence molecular imaging methods to future multi-modality imaging technology. *Theranostics*. 2014; 4: 1072-84.
27. Mao Y, Wang K, He K, Ye J, Yang F, Zhou J, et al. Development and application of the near-infrared and white-light thoracoscope system for minimally invasive lung cancer surgery. *Journal of Biomedical Optics*. 2017; 22: 66002.
28. Wang K, Chi C, Hu Z, Liu M, Hui H, Shang W, et al. Optical Molecular Imaging Frontiers in Oncology: The Pursuit of Accuracy and Sensitivity. *Engineering*. 2015; 1: 309-23.
29. He K, Chi C, Kou D, Huang W, Wu J, Wang Y, et al. Comparison between the indocyanine green fluorescence and blue dye methods for sentinel lymph node biopsy using novel fluorescence image-guided resection equipment in different types of hospitals. *Transl Res*. 2016; 178: 74.
30. Judy RP, Keating JJ, Dejesus EM, Jiang JX, Okusanya OT, Nie S, et al. Quantification of tumor fluorescence during intraoperative optical cancer imaging. *Sci Rep-Uk*. 2015; 5: 16208.
31. Lee JY, Pierce JT, Thawani JP, Zeh R, Nie S, Martinezlage M, et al. Near-infrared fluorescent image-guided surgery for intracranial meningioma. *J Neurosurg*. 2017; 1.
32. Lee JY, Thawani JP, Pierce J, Zeh R, Martinez-Lage M, Chanin M, et al. Intraoperative Near-Infrared Optical Imaging Can Localize Gadolinium-Enhancing Gliomas During Surgery. *Neurosurgery*. 2016; 79: 856.
33. Okusanya OT, Holt D, Heitjan D, Deshpande C, Venegas O, Jiang J, et al. Intraoperative near-infrared imaging can identify pulmonary nodules. *Ann Thorac Surg*. 2014; 98: 1223-30.
34. Zeh R, Sheikh S, Xia L, Pierce J, Newton A, Predina J, et al. The second window ICG technique demonstrates a broad plateau period for near infrared fluorescence tumor contrast in glioblastoma. *Plos One*. 2017; 12: e0182034.
35. Seki A, Green HR, Lee TD, Hong L, Tan J, Vinters HV, et al. Sympathetic nerve fibers in human cervical and thoracic vagus nerves. *Heart Rhythm*. 2014; 11: 1411-7.

36. Yoneya S, Saito T, Komatsu Y, Koyama I, Takahashi K, Duvollyoung J. Binding properties of indocyanine green in human blood. *Invest Ophthalmol Vis Sci.* 1998; 39: 1286.
37. Ishizawa T, Fukushima N, Shibahara J, Masuda K, Tamura S, Aoki T, et al. Real-time identification of liver cancers by using indocyanine green fluorescent imaging. *Cancer.* 2009; 115: 2491.
38. Nguyen DP, Huber PM, Metzger TA, Genitsch V, Schudel HH, Thalmann GN. A Specific Mapping Study Using Fluorescence Sentinel Lymph Node Detection in Patients with Intermediate- and High-risk Prostate Cancer Undergoing Extended Pelvic Lymph Node Dissection. *Eur Urol.* 2016; 70: 734-7.
39. Ahmed M, Purushotham AD, Douek M. Novel techniques for sentinel lymph node biopsy in breast cancer: a systematic review. *Lancet Oncology.* 2014; 15: 351-62.
40. Takashi Sakurai MD, Mariko Endo MD, Ken Shimizu MD, Nobunari Yoshimizu MD, Kenichirou Nakajima MD, Pharmacist KN, et al. Axillary reverse mapping using fluorescence imaging is useful for identifying the risk group of postoperative lymphedema in breast cancer patients undergoing sentinel node biopsies. *J Surg Oncol.* 2014; 109: 612.
41. Vorst JRVD, Schaafsma BE, Hutteman M, Verbeek FPR, Liefers GJ, Hartgrink HH, et al. Near-Infrared Fluorescence-Guided Resection of Colorectal Liver Metastases. *Cancer.* 2013; 119: 3411.
42. Degett TH, Andersen HS, Gögenur I. Indocyanine green fluorescence angiography for intraoperative assessment of gastrointestinal anastomotic perfusion: a systematic review of clinical trials. *Langenbeck Arch Surg.* 2016; 401: 1-9.
43. Keating J, Newton A, Venegas O, Nims S, Zeh R, Predina J, et al. Near-Infrared Intraoperative Molecular Imaging Can Locate Metastases to the Lung. *Ann Thorac Surg.* 2016; 103: 390-8.
44. Jiang JX, Keating JJ, Jesus EM, Judy RP, Madajewski B, Venegas O, et al. Optimization of the enhanced permeability and retention effect for near-infrared imaging of solid tumors with indocyanine green. *Am J Nucl Med Mol Imaging.* 2015; 5: 390-400.
45. Matsumura Y, Maeda H. A New Concept for Macromolecular Therapeutics in Cancer Chemotherapy: Mechanism of Tumor-tropic Accumulation of Proteins and the Antitumor Agent Smancs. *Cancer research.* 1986; 46: 6387.
46. Whitney MA, Crisp JL, Nguyen LT, Friedman B, Gross LA, Steinbach P, et al. Fluorescent peptides highlight peripheral nerves during surgery in mice. *Nat Biotechnol.* 2011; 29: 352.
47. Gibbsstrauss SL, Nasr KA, Fish KM, Khullar O, Ashitate Y, Siclovan TM, et al. Nerve-highlighting fluorescent contrast agents for image-guided surgery. *Mol Imaging.* 2011; 10: 91-101.
48. Krasna MJ. Thoracoscopic sympathectomy. *Thorac Surg Clin.* 2010; 20: 323-30.